Multifractal Simulations of the Earth's Surface and Interior: Anisotropic Singularities and Morphology

S. Lovejoy[1], D. Schertzer[2] , J.-S. Gagnon[1]

[1]Physics department, McGill University, Montréal, Canada;
E-mail: lovejoy@physics.mcgill.ca
[2]CEREVE, École Nationale des Ponts et Chaussées, Marne-la-Vallée, France

1. Abstract

Remotely sensed geodata and Geographical Information Systems attempt to quantify highly variable geofields over wide ranges of scale. We argue that the natural models for such fields are the scaling models; we show that these are all exploit the basic scaling function: the mathematical singularity; specifically, existing stochastic scaling models can all be mathematically represented as convolutions of singularities with noises of various types. We point out that due to scaling anisotropy, the basic singularity morphology can vary greatly allowing a wide variety of shapes. Concentrating on the example of the topography, we use numerical simulations to explore the often subtle interplay of singularity shape and noise type. We argue that such anistropic multifractal models provide a flexible, only weakly constraining framework for modeling geofields. In addition to topography, we give the example of the lithospheric and mantle rock density fields showing how the stratification and variability can be modeled.

2. Introduction

Geological and geophysical fields are extremely variable over wide ranges of space-time scales. Important examples are the Earth's topography and mass density which vary strongly from one location to another and from one scale to another, making it hard to tackle with classical (scale bound) geostatistics. A promising approach is to exploit scale invariant symmetries associated with power law statistics. The use of such scaling laws in topography goes back at least to Vening Meinesz (1951), who showed that the power spectrum E(k) of topography (where k is a wavenumber) roughly follows a power law $k^{-\beta}$ with a spectral exponent $\beta \approx 2$. Balmino et al. (1973), Bell (1975) followed, combining various data sets to produce a composite power spectrum that was scaling over approximately 4 orders of magnitude in scale also with a spectral exponent $\beta \approx 2$ (here and below we use the exponent of the angle integrated (not averaged) spectrum, the latter having exponent $\beta+1$). More recent spectral studies of bathymetry over scale ranges from 0.1 km to 1000 km can be found in Berkson and Matthews (1983) ($\beta \approx 1.6$-1.8), Fox and Hayes (1985) ($\beta \approx 2.5$), Gibert and Courtillot (1987) ($\beta \approx 2.1$-2.3) and Balmino (1993) ($\beta \approx 2$). Similar power law type spectra have been found by numerous authors for many other geofields including Leary (1997), Shiomi et al 1997 (borehole rock densities), Cheng 1996, 2001 (ore distributions).

If the topography has a power law spectrum, then isolines (such as coastlines) are fractal sets, they

have no tangent (Perrin (1913)) and are nonrectifiable (infinite in length; Steinhaus (1954)). In particular, Richardson (1961) found that the length of various coasts varies in a power law way with the length of the rulers used to measure it. Mandelbrot (1967), in his famous article "How long is the coast of Britain", interpreted these scaling exponents in terms of fractal dimensions. Later, with the advent of fractional Brownian motion (fBm) models of terrain (Mandelbrot (1975), Goodchild (1980)), many fractal studies on topography were made as well as the corresponding (gaussian) simulations of topography.

Since then, there have been many indirect estimates of (supposedly unique) fractal dimensions on topographic transects and surfaces using various methods to see if topography respects "fractal" statistics. The indirect methods start by postulating *a priori* that a unique fractal dimension exists, and then exploit very special monofractal relations to deduce the presumed unique fractal dimension from structure functions (variograms), power spectra or other statistical exponents (see for example Burrough (1981), Mark and Aronson (1984) for the variogram method, Gilbert (1989), Huang and Turcotte (1989, 1990) for the power spectrum method and Dietler and Zhang (1992) for the "roughening exponent" method). See also Klinkenberg and Goodchild (1992), Xu et al. (1993) and Gallant et al. (1994) for reviews and discussions of the results of such monofractal processes.

In contrast to indirect monofractal inference, direct estimates of the fractal dimension of topography and bathymetry (using box-counting for example) are surprisingly rare (see for example Barenblatt et al. (1984), Aviles et al. (1987), Okubo and Aki (1987), Turcotte (1989)). For monofractal fields (such as fBm), the box dimension is independent of the threshold used to define the set; Lovejoy and Schertzer (1990) show that for topography this is quite unrealistic. Analyzing the topography of France at 1 km resolution, they showed that the box dimension systematically decreases from 2 (the maximum possible) to 0 (the minimum) as the altitude is increased. This clearly showed that monofractals are at best an approximation of topography near the mean.

As argued in Lovejoy and Schertzer (1990) and Lavallée et al. (1993), Weissel et al. (1994), Lovejoy et al. (1995), Pecknold et al. (1997), Tchiguirinskaia et al. (2000) and Gagnon et al. (2003), it is more appropriate to treat topography as a scale invariant field, generally requiring multifractal measures and exponent functions (rather than a unique scaling exponent, such as the fractal dimension). An infinity of fractal dimensions (one for each threshold or equivalently one for each statistical moment) are then needed to completely characterize the scaling. Especially following the multifractal analyses on the large global topography data set (Gagnon et al. (2003)) - who found that the isotropic multiscaling was respected to within ±45% from planetary scales down to at least 40m - it has become more urgent to understand the significance of the result (how is it compatible with the diversity of geomorphology?), and the implications for modelling (what restrictions does it place on the types of geodynamic models we should use?). In this paper, we argue that the key is recognizing that the basic scaling function – the mathematical singularity – can itself have a bewildering variety of morphologies so that complex realistic morphologies can – at least in principle – be generated by such anistropic singulairities (on condition that they have « wild » enough statistical variability. We attempt to demonstrate this with the help of numerical simulations.

3. Singularities and Morphology

If over a range of scales, the topography has no characteristic scale, then it is natural to model it using combinations of scale invariant basis functions i.e. mathematical singularities. Perhaps the most famous such singular model is the Turcotte- Oxburg 1967 model for the variation of altitude as a function of distance from mid-ocean ridges, mathematically the form is indicated in table 1. Mandelbrot 1975 proposed a model based on the idea of making singular faults the basic shapes by summing large numbers of faults with random centers and orientations with Gaussian amplitudes; he produced a Gaussian process with long range (power law) correlations. Due to the central limit theorem (the gaussian special case), a process with the same statistical properties can be produced by using singularities of a quite different shape; table 1 (second row) indicates a model with point rather than line singularities; in this form the mathematics is more convenient for comparison with the other singular topography models summarized in table 1. In this case, in the limit of many faults, because all of the singularities have nearly the same amplitude (Gaussian variables are rarely more than a few standard deviations from the mean), the basic singularity shape is not important, we end up a rough texture but without any more interesting morphologies.

Notice in table 1 that all the stochastic models are obtained by convolutions with singularities, such convolutions are "fractional integrations" of order H' (if H'<0, there are differentiations; the difference between H, H' for fBm, fLm are necessary to take into account the scaling of the noises ϕ_2, ϕ_α). The lesson from fBm is that if we are to explain real topography by such a singular model, then the statistics of the singularities must be more extreme than gaussian so that the basic singularity shape may remain important in the limit of a large number of large singularities (i.e. after integration over the noise). One way to make some of the singularities always stand out is to use the fractional Levy motion model obtain by replacing the Gaussian noise by a Levy noise index α. The Levy random variables can be regarded as a generalization of the Gaussian variables to the case where the variance (second moment) is infinite; they have long probability tails such the statistical moments q order $q \geqslant \alpha$ and higher diverge. Due to the (generalized) central limit theorem, sums of independent (possibly weighted) Levy variables are still Levy variables. Fig. 1a shows a comparison with the corresponding fBm; several strong mountain peaks stand out; in fact, the strong peaks are too strong – although far from Gaussian - real topography empirically seems to have finite variance so this cannot be a good model.

Before moving on to the statistically and visually more realistic multifractal model, let's consider the singularity shape in more detail. The shape of line (fault-like) and point singularities depends on powers of distances from either a line or a point; in order to generalize this it turns out to be sufficient to replace the standard Euclidean distances by scale functions. Let us therefore digress a moment to discuss scale functions.

In order to change the shape of the singularities while conserving the basic statistical properties of the process, it turns out to be sufficient to make the replacement everywhere in table 1:

Table 1 An intercomparison between various models of the topography showing the essential similarities and differences in their mathematical structure, statistical properties. The deterministic Turcotte-Oxburgh model applies altitude increases to Δh from the mid-ocean ridge; their dimensional analysis gives H=1/2 (D=2 is the dimension of space). The monofractal fractional Brownian motion (fBm) model involves a fractional integration of order H' with a flux $\phi_2(x)$ which is simply a ("δ correlated") gaussian white noise with variance σ^2. Note that the symbol $a \overset{d}{=} b$ indicates equality in probability distributions, i.e. $a \overset{d}{=} b \Leftrightarrow \Pr(a > s) = \Pr(b > s)$ for all s, "Pr" indicates "probability". It results in altitude fluctuations with gaussian statistics, linear structure function exponent $\xi(q)$ and altitude independent surface codimension c (or dimension D_F). The value H=1/2 is compatible with the commonly cited value D_F= 1.5 for the level sets or D=1+1.5=2.5 for the dimension of points on the surface. The fLm is the generalization obtained by replacing Gaussian variables by stable Levy variables with index α (fBm is obtained in the case α=2). These have diverging moments q for $q \geqslant \alpha$. Finally, the multifractal Fractionally Integrated Flux model has the same structure, except that the white noises are replaced by multifractal noises ϕ_λ where λ is the resolution. The multifractal noise ϕ_λ is the result of a continuous in scale multiplicative cascade, mathematically it is given by $\Gamma_\lambda(\vec{x}) \propto \int_1^\lambda \frac{\gamma_\alpha(\vec{x}')}{|\vec{x}-\vec{x}'|^{D-H'}} d\vec{x}'$; $\phi_\lambda(\vec{x}) = e^{\Gamma_\lambda(\vec{x})}$; $H' = D(1-1/\alpha)$; $\gamma_\alpha(\vec{x})$ = independent Levy noise, index α, amplitude depends on C_1, Γ_λ is an fLm process called the "generator". It is multiplicative because of the exponentiation of the additive process Γ: $\phi = e^\Gamma$. We again find H≈1/2, although now there are an infinite number of codimensions c(γ) (or dimensions $D_F(\gamma)$) that depends on the threshold given by λ^γ. (γ is an order of singularity; not to be confused with the subgenerator γ_α). In all cases, H can in principle be determined by dimensional analysis so that the Turcotte- Oxburgh exponent H=1/2 may be valid for all the models, c.f. [*Lovejoy*, 1995]. To generalize fBm, fLm and FIF to anisotropic topographies, we must replace the distances in the fractional integration denominators by anisotropic scale functions as discussed in the text.

Altitude model	Altitude with corresponding noise statistics	Resulting statistics of altitude fluctuations	Codimension (c), dimension (D_F) level sets
Deterministic Mid-ocean ridge	$h(\vec{x}) = \int \frac{\delta(\hat{r}\cdot(\vec{x}'-\vec{x}_0))}{|\hat{r}\cdot(\vec{x}-\vec{x}')|^H} d\vec{x}'$ δ=Dirac delta function, $\hat{r}$ is a unit direction vector, $\vec{x}_0$ through $\vec{x}_0$. No noise statistics (deterministic)	$\Delta h \propto \lvert\Delta\vec{x}\rvert^H$ No altitude statistics (deterministic)	c=1, D_F=1
Stochastic Monofractal fBm	$h(\vec{x}) = \int \frac{\phi_2(\vec{x}')}{|\vec{x}-\vec{x}'|^{D-H'}} d\vec{x}'$ $H' = H + D/2$, $\phi_2(\vec{x})$ = independent Gaussian white noise, D=2	$\Delta h \overset{d}{=} \phi \lvert\Delta\vec{x}\rvert^H$, $\langle \Delta h^q \rangle \propto \lvert\Delta\vec{x}\rvert^{\xi(q)}$, with $\xi(q) = qH$	$c = H$ $D_F = D - c$

Stochastic Monofractal fLm	$h(\vec{x}) = \int \frac{\phi_\alpha(\vec{x}')}{\lvert \vec{x} - \vec{x}' \rvert^{D-H'}} d\vec{x}'$ $H' = H + D/\alpha$ $\phi_\alpha(\vec{x})$ = independent Levy noise index $0 \le \alpha \le 2$ D=2	$\Delta h \overset{d}{=} \phi_\alpha \lvert \Delta \vec{x} \rvert^H$ $\langle \Delta h^q \rangle \propto \lvert \Delta \vec{x} \rvert^{\xi(q)}$ $\xi(q) = \begin{cases} qH; & q < 1/\alpha \\ \infty; & q > 1/\alpha \end{cases}$	$c = H$ $D_F = D - c$
Stochastic Multifractal FIF	$h_\lambda(\vec{x}) = \int \frac{\phi_\lambda(\vec{x}')}{\lvert \vec{x} - \vec{x}' \rvert^{D-H'}} d\vec{x}'$ $H' = H$ λ = range of scales, D=2	$\langle \phi_\lambda^q \rangle = \lambda^{K(q)}$ $K(q) = \frac{C_1}{\alpha - 1}(q^\alpha - q)$ $0 \le \alpha \le 2$ $\Delta h = \phi_\lambda \lvert \Delta \vec{x} \rvert^H$, $\langle \Delta h^q \rangle \propto \lvert \Delta \vec{x} \rvert^{\xi(q)}$, with $\xi(q) = qH - K(q)$	$c(\gamma) = \max_q (qH - K(q))$ $D_F(\gamma) = D - c(\gamma)$

$$\lvert\ \rvert \to \left\| \vec{x} - \vec{x}' \right\|; \quad D \to D_{el} \tag{1}$$

i.e. to replace the usual distance ("$\lvert\ \rvert$") by a "scale function" ("$\|\ \|$") and usual dimension of space by an "elliptical dimension" D_{el} which satisfies the following basic equation scaling:

$$\left\| T_\lambda \vec{x} \right\| = \lambda^{-1} \left\| \vec{x} \right\|; \quad T_\lambda = \lambda^{-G}; \quad D_{el} = TraceG \tag{2}$$

where T_λ is a scale changing operator which reduces the scale of a vector by a factor λ. In order for the scale function to be scaling (i.e. have no characteristic scale), it must satisfy group properties, hence it must admit a generator G as indicated. Once all the unit vectors $\vec{x}_1$ are specified the scale eq. 2 uniquely specifies the scale of all vectors; all the nonunit vectors ($\left\| \vec{x}_\lambda \right\| = \lambda; \quad \lambda \neq 1$) are then generated by the action of T_λ: $\vec{x}_\lambda = T_\lambda \vec{x}_1$ (see [*Schertzer and Lovejoy*, 1985] for technical details on this Generalized Scale Invariance, GSI). The set of all vectors $\left\| \vec{x} \right\| \le \lambda$ is called a "ball", denoted B_λ; for physical scale functions B_λ must be strictly decreasing (i.e. $B_{\lambda'} \subseteq B_\lambda; \quad \lambda' < \lambda$). We can see that if the replacements $\left| \vec{x} - \vec{x}' \right| \to \left\| \vec{x} - \vec{x}' \right\|; \quad D \to D_{el}$ are made in the denominators of the models in table 1, with scale functions satisfying the scale eq. 2 (in fact they then define the notion scale) then the convolutions will have power law dependencies under "zooming", i.e. the models will be scaling as long as the noises are also scaling (hence the special choices of Gaussian or Levy noise, or in the multifractal case, multifractal noise).

When scale functions are used as the basic singularities, the shapes can be extremely varied, hence demonstrating the possibility of modeling geomorphologies in this way. First consider G = the identity: the resulting models will be "self-similar" in the sense that their statistics will vary in power law ways under isotropic "zooming" (blow-ups). When the unit ball is a circle (or more generally a

D dimensional sphere), then we obtain $\|\vec{x}\| = |\vec{x}|$. However when the unit ball is not circular (spherical), then there will still be preferred directions. These preferred directions will be the same at all scales, the anisotropy is "trivial" (see fig. 6a for examples). Things become more interesting as soon as G is no longer the identity. If G is a diagonal matrix, then the singularities order γ: $\|\vec{x}\|^{-\gamma}$ are quite different in different directions, the resulting fractals/multifractals are "self-affine". The case where G is nondiagonal and the eigenvalues are real is a generalization in which the main stretching/shrinking occurs along nonorthogonal eigendirections; Fig. 1a,b shows the resulting differential stratification. When the eigenvalues are complex, then the eigenvectors rotate continuously as functions of scale (fig. 3). Finally, we can consider noncircular/nonspherical unit balls, fig. 1a,b shows how the basic singularity shapes are clearly visible in the fLm. In the multifractal case, the effect of the singularity morphology is still important for the result; but things are more subtle. Fig. 2a, b shows the effect of changing the scale function while maintaining the G, and fig. 3 shows that even spiral shaped singularities can be used. Finally - outside our present scope but presumably important for realistic topography modelling – we can consider G as a nonlinear operator (rather than a matrix). In this case, the anisotropy depends not only on scale but also on the location. This allows for spatially varying morphologies. In this case, the linear GSI discussed above in simply a locally valid approximation.

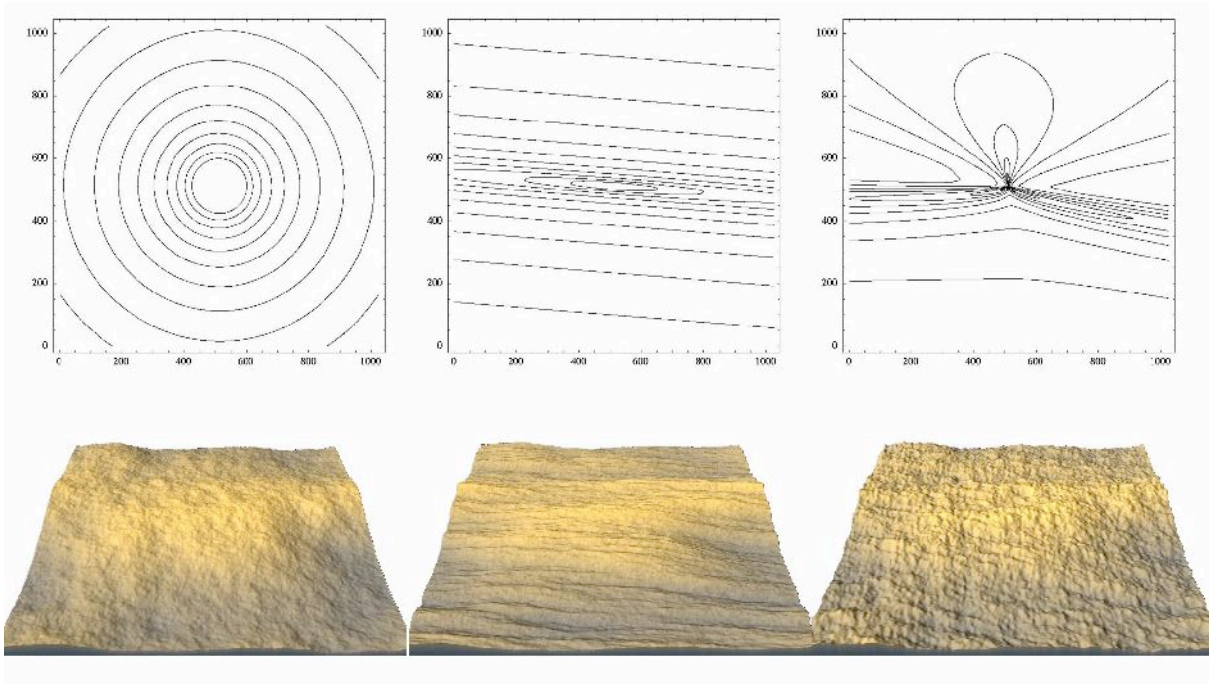

Fig. 1a. This shows scale functions (top row and fBm bottom row with parameter H=0.7 (corresponding to continental statistics; see below). From left to right, we change the anisotropy. Left is self-similar (isotropic), right two are symmetric with respect to $G = \begin{pmatrix} 0.8 & -0.05 \\ 0.05 & 1.2 \end{pmatrix}$. In the middle, the unit ball is circular at 1 pixel, at right, It has the form $r(\theta)=1+0.65\ \mathrm{Cos}(3\theta)$. In the fBm, one mainly perceives textures, there are no very extreme mountains or other morphologies evident.

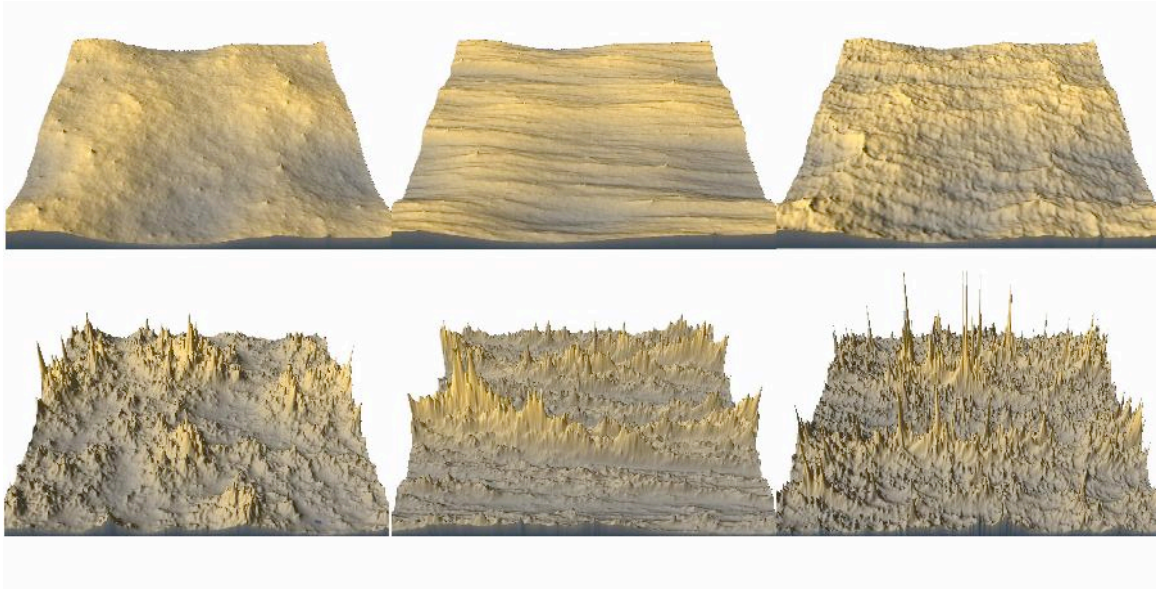

Fig. 1b. Same scale functions as 1a except top row is fLm with α=1.8, H=0.7 and bottom row is a multifractal simulations with (roughly) the observed parameters (see below; α=1.8, C_1=0.12, H=0.7), One can see that the fLm is too extreme, the shape of the singularity (particularly visible in the far right) is quite visible in the highest mountain shapes (a technical point: in the fLm we used maximally skewed Levy variables, hence the absence of pointed "holes" i.e. all the extreme singularities are positive). The multifractal simulation is more realistic in that there is a more subtle hierarchy of mountains.

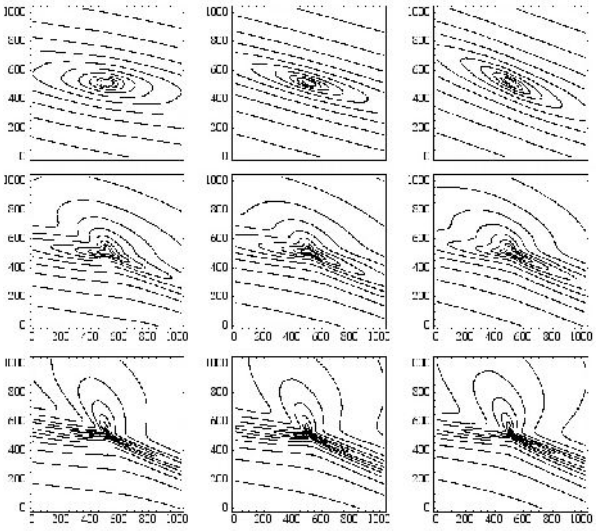

Fig. 2a. This figure shows the effect of changing the shape of the scale functions for $G = \begin{pmatrix} 1.2 & -0.1 \\ 0.1 & 0.8 \end{pmatrix}$. The unit vectors are defined by the polar coordinate formula: $r = 1 + a\cos(3(\theta - \theta_0))$.

The rows top to bottom have a=0.1, 0.5, 0.85, the columns, left to right have θ_0=0, π/4, π/2.

In spite of the systematic finding of scaling or near scaling statistics, many geophysicists instinctively reject all wide range scaling; for example Herzfeld et al. (1995) and Herzfeld and Overbeck (1999). They argue that the ocean floor (and topography in general) cannot be scaling over a wide range of scales, because of their conviction that geomorphologic processes are scale dependent (i.e. necessarily have characteristic lengths): they consider *a priori* that the scaling is broken.

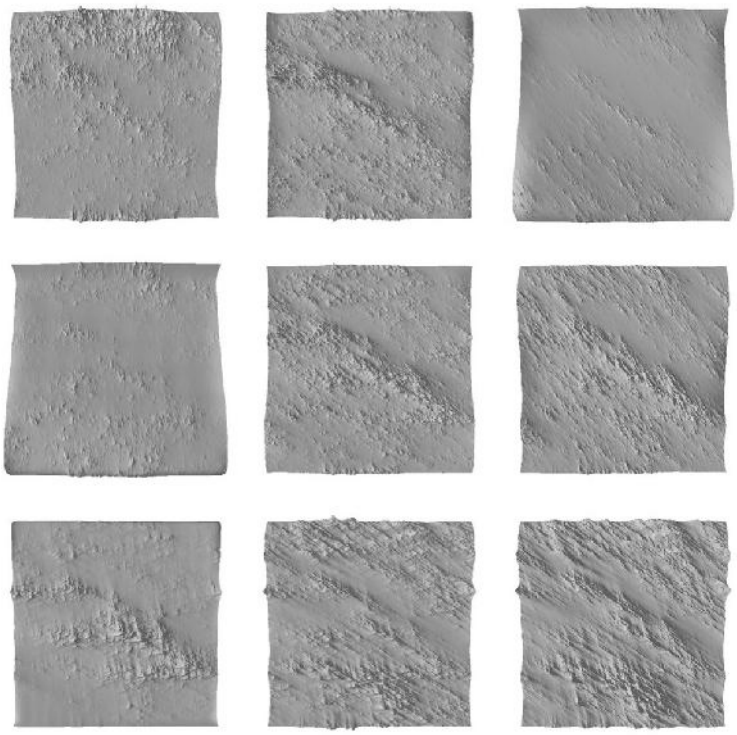

Fig. 2b. These are the multifractal simulations (same seeds so that the structures can be compared) with multifractal parameters α=1.8, C_1=0.12, H=0.7 and the scale functions from fig. 2a.

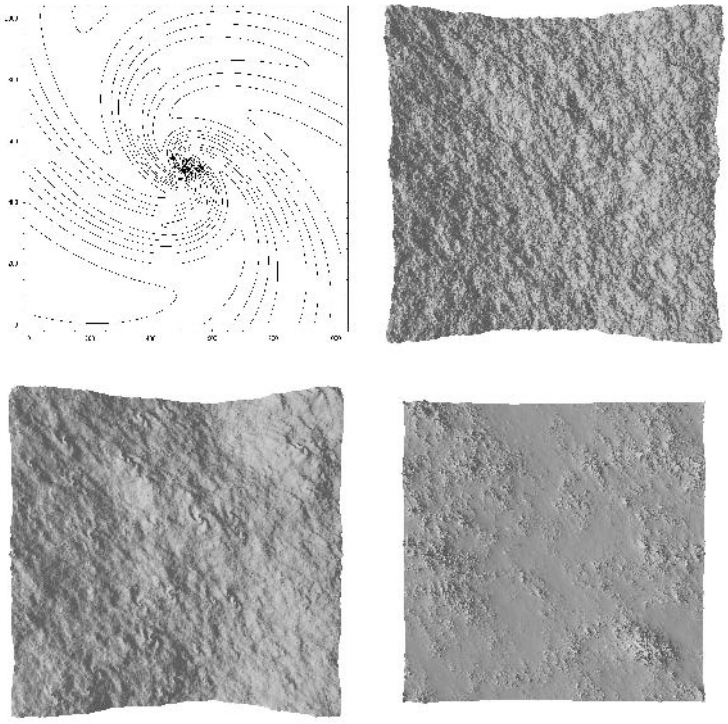

Fig. 3. This simulation (with $G = \begin{pmatrix} 0.5 & -1.5 \\ 1.5 & 1.5 \end{pmatrix}$, i.e. complex eigenvalues; eigenvectors rotate with scale) shows how the use of spiral singularities (scale function upper left) does not affect the fBM (upper right), leads to too strong singularities for the fLm (lower left), but subtle variations of mountains and plains for the multifractal (lower right; the three simulations have the same statistical parameters as in the previous).

They have attempted to demonstrate this by estimating power spectra and variograms on a few bathymetry transects which they showed to have poor scaling. Rather than giving a purely theoretical explanation as to why their results are not so surprising and how they might be compatible with the scaling hypothesis, let us consider a simulation of their transect, fig. 4 (about the same length; 1024 points).

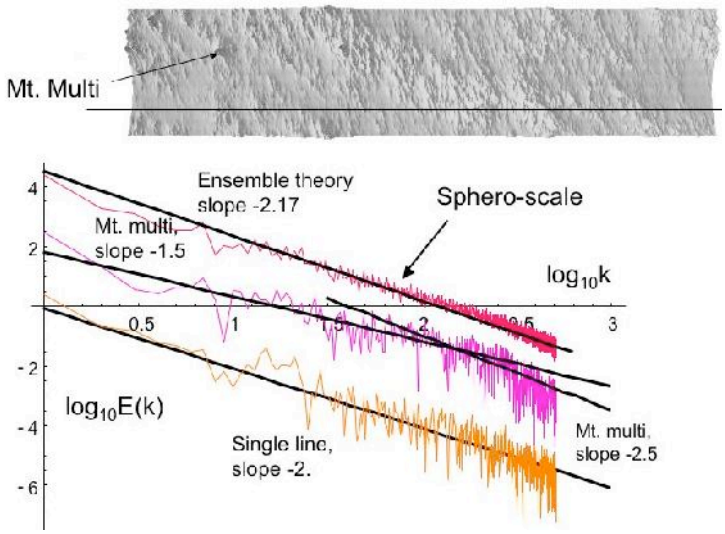

Fig. 4. A simulated bathymetry transect. The parameters are $G=\begin{pmatrix} 0.7 & -0.02 \\ 0.02 & 1.3 \end{pmatrix}$, α=1.9, C_1=0.12, H=0.7. The energy spectra of the transect passing through "Mt. multi" (the highest peak in the simulation), and through another (randomly chosen) transect are shown as well as the ensemble over all the transects.

The figure compares the energy spectra of two individual transects as well as the ensemble over all the transects. One of the transects passes through "Mt. Multi", the highest peak in the range, another through a randomly chose transect not far away. One can see that the Mt. Multi scaling is pretty poor; a naïve analysis would indicate two ranges with a break at about 10 pixels with high frequency exponent β=2.5, low frequency β=1.5 (this is a large change in spectral slope). Clearly this break has nothing to do with the scaling of the process (which is perfect except due - to finite element effects - for the highest factor of two or so in resolution).

In comparison, the randomly chosen transect has better scaling, but with $\beta \approx 2$. In comparison, the isotropic (i.e. angle averaged) spectrum averaged over an infinite ensemble of realizations has β=2.17. Even the average over the transects shows signs of a spurious break at around 16 pixels (the scale where the north-south and east west fluctuations are roughly equal in magnitude, the "sphero-scale"); this explains why the theory line does not pass perfectly through the curve corresponding to the average of the transects. Clearly, since a priori, the physically relevant notion of scale in not known, the first task should be to determine it (with the matrix G). However, this is still a difficult unsolved problem (see however Lewis et al 1999). Obviously, even for fixed parameters, had we chosen a different random seed, the results for the individual transects would have been somewhat different (even the average over the transects would have been a bit different), see the example in the next section.

Conclusions about broken scaling in fig. 4 are therefore erroneous. Perhaps the most important reason for this misinterpretation is that scale invariance is a statistical symmetry which is almost surely broken on every single realization, hence it is important to have a large data base (i.e. large range of scales, many realizations) to average fluctuations and approximate the theoretically predicted ensemble scaling. In fact, due to the singularities of all orders (see previous section) the variability of multifractals is much greater than that of classical stochastic processes; for example, rare (extreme) singularities are produced by the process yet they are almost surely absent on any given realization. This means that they do not have the property of "ergodicity". What may be nothing more than normal multifractal statistical variability can thus easily be interpreted as breaks in the scaling. A second reason for the error is the assumption that the scaling is isotropic so that breaks in statistics on 1-D subspaces (transects) do not imply that the full process is not scaling. A third reason discussed a bit more below is that there can be systematic biases due to the use of conditional statistics (such studying the transect that happens to pass through a special feature such as Mt. Multi, rather than a randomly chosen transect).

The strong singularities in multifractals leads to apparent nonstationarities: e.g. quite different morphologies often in close proximity. This is often interpreted in terms of nonstationarities – different processes at work in different regions or at the very least, variations in the parameters of a single basic model. However, with multifractals such interpretations would be unwarranted: the basic multifractal processes are statistically stationary/homogeneous in the strict sense that over the region over which they are defined (which is necessarily finite), the ensemble multifractal statistical properties are independent of the (space/time) location (and this, for any spectral slope β). Rather thandiscussing this at an abstract level, let us see what happens when we analyse a self-similar 1024X1024 multifractal simulation (fig. 5a). Fig. 5b shows the compensated (i.e. $k^{2.17}E(k)$), isotropic spectrum obtained by integrating the fourier modulus squared over circles radius k in fourier space.

The low frequencies are quite flat indicating that the simulation has roughly the ensemble spectrum as expected. At high frequencies, there is a drop off which is an artifact of the numerical simulation techniques. We can now consider the “regional” variability in the spectral exponent β by dividing the simulation into 8X8 squares, each with 128X128 pixels. Fig. 5c (left) shows the histogram of the 64 regression estimates of the compensated spectra: the mean is close to zero as expected, but we see a large scatter implying that there are some individual regions having β as low as 1.2, some as high as 2.7; the standard deviation is ±0.3. As we shall see later, this would imply a random variation in local estimates of H of ±0.3/2=±0.15 (which is of the order of the difference observed between continents and oceans, although this spread in β, H will decrease as the size of the data set increases). In fig. 5c, we can also see the large variations in the log prefactors ($\log_{10}E_1$; $E(k)=E_1k^{-\beta}$). If this is interpreted in terms of roughness, the roughest of the 64 regions has about 10^3 times the variance as the smoothest. While it would obviously be tempting to give different interpretations to the parameters in each region, this would be a mistake. On the other hand, this does not imply that the roughest and the smoothest would be associated with identical erosional, orographic or other processes, the point is that in a full coupled model, that these processes would be also be scaling and

would have correlated variations. Fig. 5 also demonstrates the fact that if data from special locations (such as near mountains) are analysed that we may expect systematic biases in our statistics and parameter estimates. This is discussed quantitatively in Lovejoy et al 2001. This underlines the need for coupled multifractal processes, possible through the use a state vector and vector mulitfractal processes ("based on "Lie cascades", see [*Schertzer and Lovejoy*, 1995], Lovejoy et al 2001).

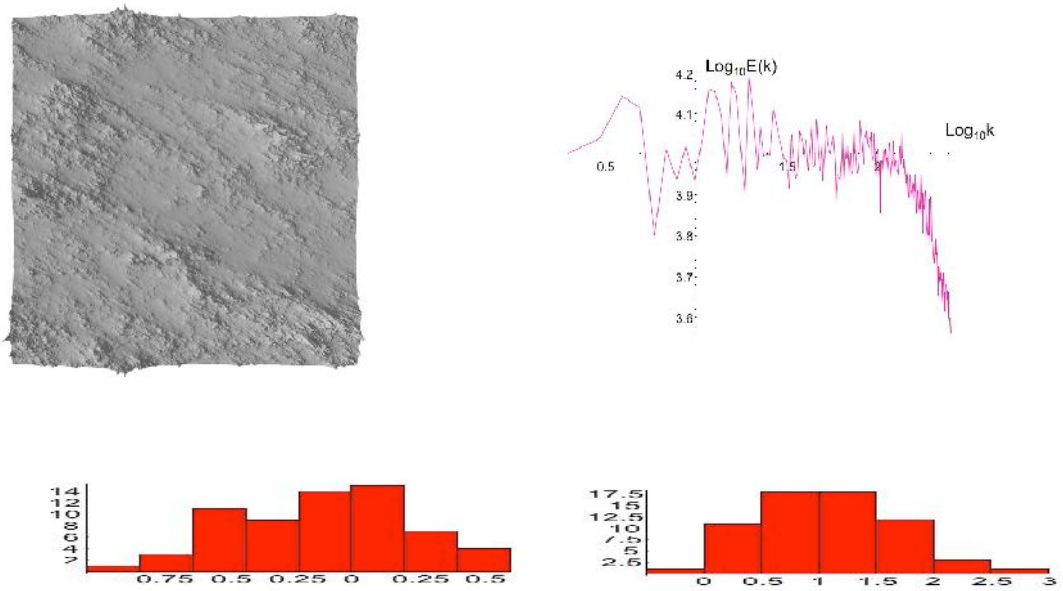

Fig. 5. (Upper left): This is a 1024X1024 self-similar simulation with some trivial anisotropy, α=1.9, C_1=0.12, H=0.7, hence β=1+2H-K(2)=2.17. (Upper right): Compensated spectrum, β=2.17 (the extreme factor 2 in wavenumber fall-off too rapidly. This is an artifact due to the difficulty of discretising singularities on numerical grids). (Lower left): After dividing fig. 5a into 64 128X128 squares, we calculated the isotropic spectrum in each, and fit the slope to the lowest factor 16 in scale (we remove the highest factor 4 due to numerical artifacts at the highest wavenumbers). The resulting $\Delta\beta$ is given in the left; it is twice the ΔH, showing that H can vary by 0.5 over a single region. (Lower right): A histogram of the $\log_{10}E_1$ (E_1 is the spectral prefactor: $E(k)=E_1k^{-\beta}$) showing variation of 1000 from the smoothest to roughest subregion.

5. The effect of the multifractal parameters H, C1, α:

From table 1 we see that for a (universal) multifractal at a given (generally anisotropic) resolution λ (defined by the appropriate anisotropic scale function); we have:

$$\left\langle \left| \Delta h\left(\underline{\Delta r}\right) \right|^q \right\rangle = \left\| \Delta r \right\|^{\xi(q)}; \quad \xi(q) = qH - K(q); \quad K(q) = \frac{C_1}{\alpha - 1}(q^\alpha - q) \tag{3}$$

(Although for a general multifractal K(q) need only be convex, Schertzer and Lovejoy (1987, 1997) have shown that there exists a class of stable and attractive multifractal processes called "universal multifractals" whose two parameter form is given on the right). α and C_1 are the two basic parameters characterizing the scaling properties of the multifractal noise ϕ_λ. The parameter C_1 is the fractal codimension of the set giving the dominant contribution to the mean (q=1). For a 2-D process such as topography, it varies from 0 to 2. The value C_1=0 implies that the set giving the dominant

contribution to the mean is space filling (i.e. its fractal dimension is equal to the one of the embedding space), so it can be interpreted as quantifying the sparseness of the mean field. The parameter α is the degree of multifractality and varies from 0 to 2, where 0 is the monofractal special case. It describes how rapidly the fractal codimension (sparseness) of sets at different thresholds decrease as we move to more and more extreme values (singularities); the larger α, the more rapid the change. As it is not very intuitive; the accompanying simulations may be the best way to visualize the effect of varying α (see Fig.6).Many more simulations can be found at the multifractal explorer web sit ehttp://www.physics.mcgill.ca/~gang/multifrac/index.htm.

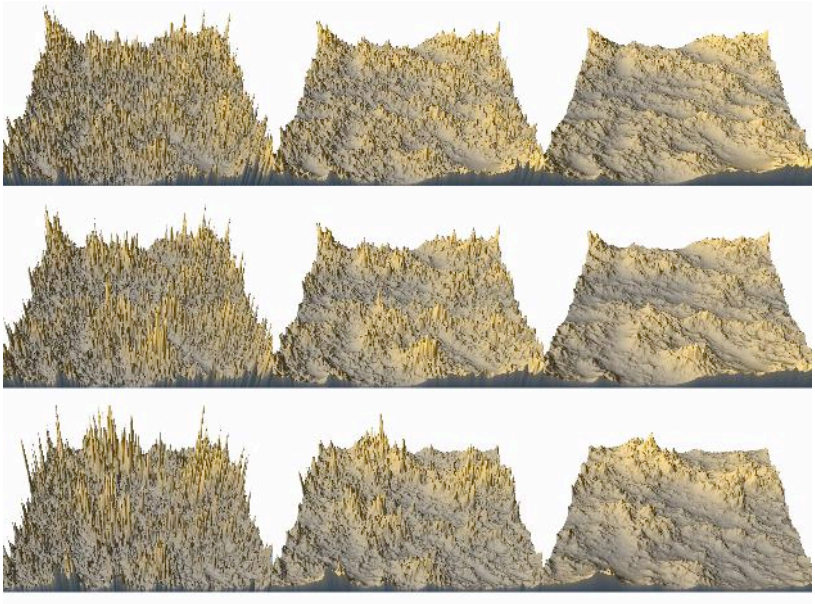

Fig. 6a. This shows the effect varying α, H on self-similar multifractals with C_1=0.1 (there is some trivial anisotropy, the random seed is the same in all cases). From left to right, H=0.2, 0.5, 0.8, from top to bottom, alpha varies from 1.1, 1.5, 1.9. As H increases, the fields become smoother, as α decreases, one notices more and more prominent "holes" i.e. low smooth regions. The realistic values correspond to the two lower right hand simulations.

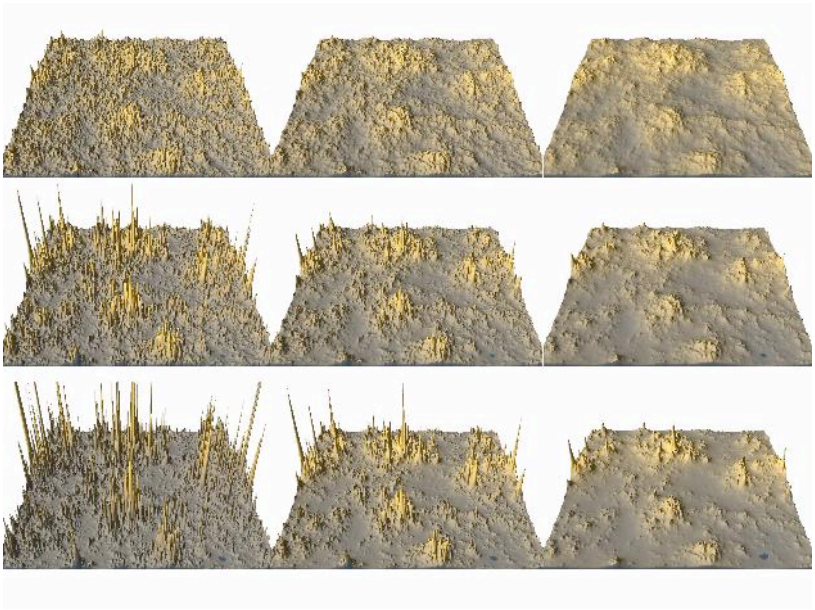

Fig. 6b. Self-similar simulations (no trivial anisotropy) with α=1.8 with C_1 varying from 0.05 to 0.15, 0.25 (top to bottom), H varying from 0.2 to 0.5 to 0.8 (left to right). Increasing H smoothes the fields, increasing C_1 makes the sets exceeding a high thresholds more sparse.

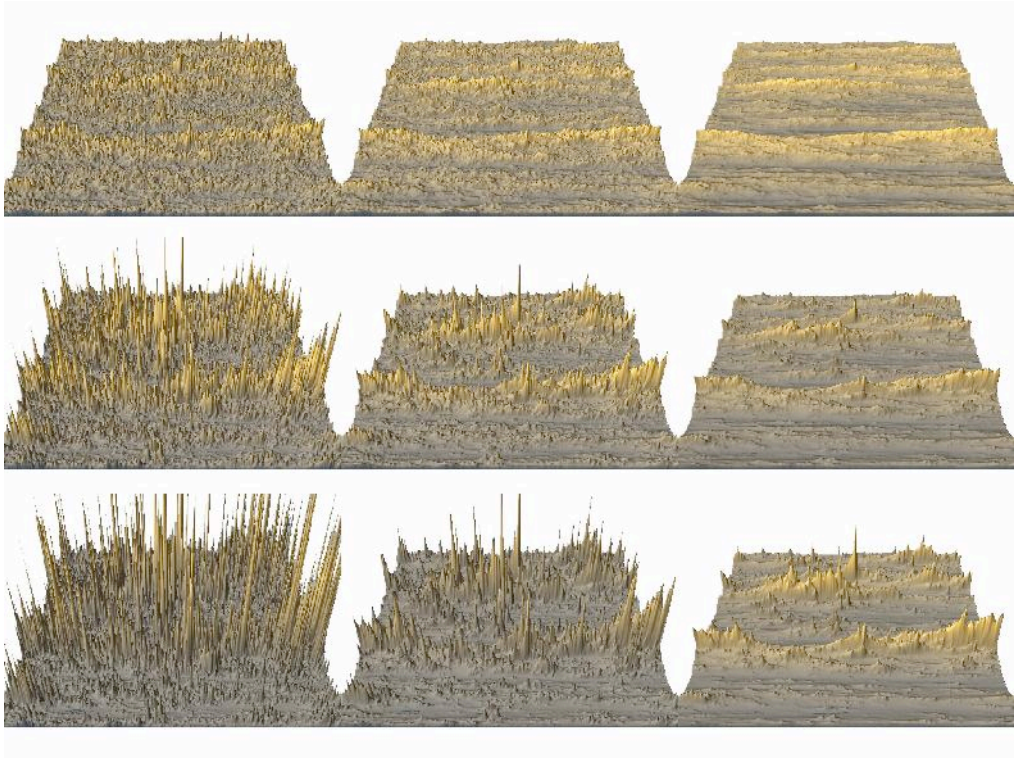

Fig. 6c. This shows self-affine simulations with α=1.8, C_1 increasing top to bottom (0.05, 0.15, 0.25), H=0.2, 0.5, 0.8 left to right, $G=\begin{pmatrix} H_x & 0 \\ 0 & H_z \end{pmatrix}$, H_x=1.2, H_z=0.8 (sphero-scale= 1 pixel, same seed in all the simulations). The middle row two far right correspond the closest to the data. If only 1-D transects were available in the up down (z) or left-right (x) directions, different exponents would be found. For example the spectral exponents would be related as: $(\beta_x-1)/H_x=(\beta_z-1)/H_z$. The structure function exponents (ξ(q)) and trace moment exponents (K(q)) would also be in the ratio of the H's: $\xi_x(q)/\xi_z(q)=K_x(q)/K_z(q)=H_x/H_z$.

6. Multifractal Simulations of The Mantle and Lithospheric Rock Densities

Up until now, we have concentrated our discussion on the topography field, partly because of its long history of scaling analyses and modeling but also because of its importance and the relative ease with which simulations can be visualized using standard ray tracing techniques. If the topography is scaling over wide ranges, then it is quite plausible that other geodynamic processes are also scaling. Following this idea, Lovejoy et al 2001 and Pecknold et al 2001 have shown that the magnetic susceptibility is scaling over wide ranges in the horizontal and in the vertical (boreholes) down to the Curie depth; they used this to explain the surface magnetic field fluctuations out to thousands of kilometers in scale in the horizontal. In order to do so, they showed that the susceptibility (M) must be quite stratified in the vertical, specifically, they estimated that for the horizontal-vertical (x,z) plane, that $G=\begin{pmatrix} 1 & 0 \\ 0 & 1.7 \end{pmatrix}$ implying that at very large scales structures in the susceptibility field were vertically aligned, while at smaller scales, they were horizontally stratified, with the transition occurring at the sphero-scale estimated to be around 2000km (note that this is the opposite of the atmospheric stratification which becomes flatter at larger scales with $G=\begin{pmatrix} 1 & 0 \\ 0 & 5/9 \end{pmatrix}$, c.f. Lilley et al 2004). The

multifractal parameters for M were H=0.2, C_1=0.1, α=1.9. A similar analysis Lovejoy et al 2001b (EGS) of the lithospheric density field as estimated by both horizontal and vertical boreholes gives $G = \begin{pmatrix} 1 & 0 \\ 0 & 3. \end{pmatrix}$ with a sphero-scale of about 220km; from published spectra we

Finally, the parameter H is the degree of "nonconservation" of the observed field $\left\langle \left| \Delta h\left(\vec{\Delta r}\right) \right| \right\rangle = \left\| \vec{\Delta r} \right\|^H$

(the jargon comes from multifractal cascade models; H can be interpreted as a degree of smoothness it is unconstrained, the higher H the smoother the field; see Fig. 6). See table 2 for various empirical analyses of the topography.

Table 2 Universal multifractal parameters for various topographic data sets. The ETOPO5 is a global data set; the parameters α=1.8, C_1=0.12 fit well everywhere; the H parameter seems to vary from about 0.45 to 0.75 from continents to oceans, see Gagnon et al 2003.

Data sets	Horizontal resolution	Regions analyzed (in pixels)	β	α	C_1	H	References
ETOPO5	≈10 km	2160x4000	2.12	1.81	0.13	0.69	Gagnon et al (2003)
GTOPO30	≈1 km	1225x4096	2.04	1.77	0.08	0.60	Gagnon et al (2003)
U.S.	90 m	2500x65536	2.08	1.51	0.09	0.61	Gagnon et al (2003)
Lower Saxony	50 cm	3000x6000	1.86	2.00	0.17	0.60	Gagnon et al (2003)
Deadman's Butte	50 m	512x512	1.93	1.9	0.045	0.51	Lavallée et al.(1993)
French topography	1 km	512x512	---	1.7	0.075	---	Lavallée et al.(1993)
U.S.	90 m	20 x 512x512	1.91	1.70	0.07	0.52	Pecknold et al.(1997)

estimate H_ρ=0.2. The density is therefore a little more differentially stratified but has the same qualitiative behaviour as the susceptibility; using the same C_1, α as for susceptibility, we obtain the crust density simulation shown in fig. 7a. Simulations such as these can be used to simulate the surface gravity field if the lithospheric/mantle boundary, topography are also modelled.

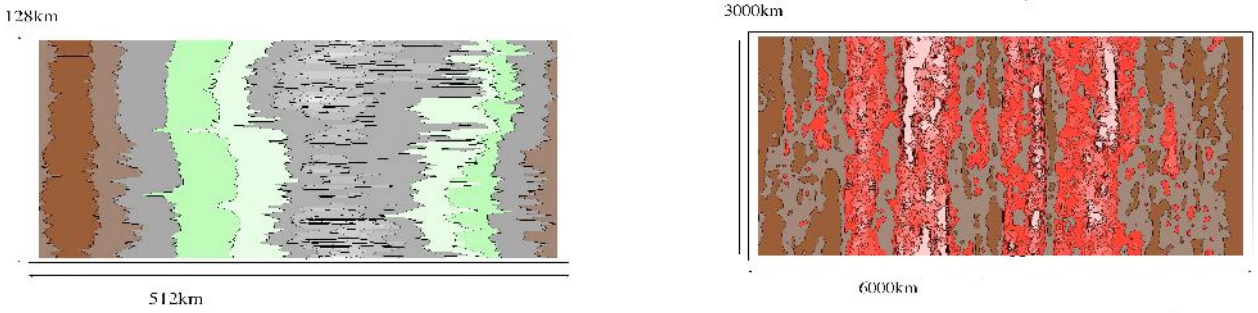

Fig. 7. (Left) This simulation of the lithospheric rock density has a 2:1 aspect ratio and sphero-scale l_s=256km, with 1 pixel -1km. The parameters are α=1.8, C_1=0.1 $G = \begin{pmatrix} 1 & 0 \\ 0 & 3. \end{pmatrix}$. (Right): The above is a mantle simulation with sphero scale = 1 pixel parameters are α=1.8, C_1=0.1,H= -1, $G = \begin{pmatrix} 1 & 0 \\ 0 & 3. \end{pmatrix}$. Each pixel is 50 km, so that a sphero-scale of 25km. Hot (low density) plumes shown as white/red (this is a model for either density or temperature fluctuations (the two being proportional; we assume constant expansion coefficient). These are for fluctuations with respect to the mean vertical profile.

In order to get an idea of the mantle density variability due to highly nonlinear mantle convection, we appealed to dimensional analysis of the fluid equations (high Prandtl number). There are three key fluid equations: the velocity equation, the temperature equation and the heat equation. Each equation depends respectively on the dimensional combinations $g\alpha/\nu$, $Q/c_p\rho_0$, where Q is the heat flux, ν the viscosity, ρ_0 the average density, g the acceleration of gravity c_p the heat capacity, κ the thermal conductivity. From these we obtain unique length scales, time scales and temperature scales:

$$l_s \approx \left(\frac{\rho_0 c_p \nu \kappa^2}{g\alpha Q} \right)^{1/4} \qquad \tau_s \approx \left(\frac{c_p \rho_0 \nu}{Q g \alpha} \right)^{1/2} \qquad T_s \approx \left(\frac{Q^3 \nu}{g\alpha \rho_0^3 c_p^3 \kappa^2} \right)^{1/4} \tag{4}$$

Using estimated mantle values, we find l_s=20km, $\tau_s=10^7$ yrs, T_s=375K. Also from dimensional analysis, we can derive typical density fluctuations: ρ_s=30Kg/m^3, v_s=2mm/yr. In order to understand the significance of these values, we need to know how fluctuations varying with scale in both horizontal and vertical directions. Using an analysis of the equations and empirical laboratory results on thermal plumes (C. Jaupard, private communication), we can deduce:

$$\Delta\rho(\Delta x) = \rho_s \left(\frac{\Delta x}{l_s} \right)^{-1}; \quad \Delta\rho(\Delta z) = \rho_s \left(\frac{\Delta z}{l_s} \right)^{-1/3} \tag{5}$$

(with analogous results for the vertical component of the velocity and also for the temperature). From eq. 5, we can see that the two equations can be combined:

$$\Delta\rho\left(\vec{\Delta x}\right) = \rho_s \left(\frac{\left\| \vec{\Delta x} \right\|}{l_s} \right)^H \tag{6}$$

where the scale function is symmetric with respect to the matrix $G = \begin{pmatrix} 1 & 0 \\ 0 & 3. \end{pmatrix}$ and H = -1. The negative value of H implies that fluctuations decrease with scale rather than increase (which is much more usual), but this is in accord with the idea that the convection homogenizes the mantle at very large scales. From this we see that the interpretation is that the smallest scale of the heterogeneity is around l_s (20km), ρ_s, T_s are the typical fluctuations at that scale (these are fluctuations with respect to mean vertically varying temperature and density profiles). Extrapolating eq. 5 to horizontal scales of 3000km, we find that the typical variations are very reasonable. Using the same α, C_1 as before, we therefore obtain the simulation in fig. 7b. We see that qualitative features such as hot columnar structures ("plumes") are evident. Elsewhere, we explore this in more detail and –with the help of such multifractal models -examine the consequences for the surface gravity field.

7. Conclusion

Geological and geophysical systems are typically nonlinearly variable over huge ranges of space-time scales. Traditional scale-bound models and geostatistics are only useful for characterizing and/or modelling the variability over one or perhaps two orders of magnitude in scale. In order to extend this to the much larger geodynamically relevant ranges of scales - which in the (typical) case of the topography and rock densities – spans the range from planetary down to millimetric (or smaller) scales, spectral analysis and other fractal and multifractal analyses and models are necessary. For

example, starting with Venig-Meinsz 1951, such methods have now shown that over the range of planetary down to at least 40m the basic isotropic scaling of the topography is respected to within ±45% (Gagnon et al 2003).

The corresponding models (including the deterministic ocean ridge Oxburgh-Turcotte model) all built using the basic scaling function – mathematical singularities. Singularities have strengths which fall-off much more slowly than the exponentials of the scale bound models, and are associated with large (but possibly random) structures, morphologies. In addition, we show that the stochastic scaling models (fractional Brownian motion, fractional Levy motion, the multifractal fractionally integrated flux model), are all convolutions of noises with singularities (called "fractional integrations") so that the resulting morphologies depend on both the statistical properties of the underlying noise, as well as the shape of the singularities. After a long period of debate, it has now become clear – for the topography at least – that the underlying noise is a multifractal. In this paper, we showed (with the help of Generalized Scale Invariance) how the resulting morphology depended not only on the basic multifractal parameters, but equally importantly – on the shape of the (generally) anisotropic singularities. We presented a series of simulations so as to visually demonstrate that wildly different geomorphologies can be compatible with scaling statistics. These strong singualirites have several nonclassical statistical features which often makes conventional intuition a poor guide; we demonstrated how spurious breaks and nonstationarities can arise.

Rather than being a straightjacket restricting the types of geodynamical model we argue that on the contrary scaling provides a broad framework *a priori* consistent with the observed morphologies and required by and increasing number of isotropic statistical analyses. Although we focused on the important case of the earth's topography, we also indicated how realistic simulations of lithospheric and mantle rock densities can be made.

8. References

Aviles, C. A., C. H. Scholz and J. Boatwright, 1987. Fractal analysis applied to characteristic segments of the San Andreas fault. *J. Geophys. Res.*, 92, B1, 331-344.

Balmino, G., K. Lambeck and W. Kaula, 1973. A spherical harmonic analysis of the Earth's topography. *J. Geophys. Res.*, 78, 2, 478-481.

Balmino, G. , 1993. The spectra of the topography of the Earth, Venus and Mars. *Geophysical Research Letters*, 20, 11, 1063-1066.

Barenblatt, G. I., A. V. Zhivago, Y. P. Neprochnov and A. A. Ostrovskiy, 1984. The fractal dimension: a quantitative characteristic of ocean-bottom relief. *Oceanology*, 24, 6, 695-697.

Bell, T. H. , 1975. Statistical features of sea-floor topography. *Deep-Sea Research*, 22, 883-892.

Berkson, J. M. and J. E. Matthews, 1983. Statistical properties of sea-floor roughness, in *Acoustics and the Sea-Bed*, edited by N. G. Pace, pp. 215-223, Bath University Press, Bath, England.

Burrough, P. A. , 1981. Fractal dimensions of landscapes and other environmental data. *Nature*, 294, 240-242.

Cheng, Q., Agterberg, F.P. and Bonham-Carter, G.F., 1996. Spatial analysis method for geochemical anomaly separation, *Journal of Exploration Geochemistry*, v. 56, no. 3, p. 183-195.

Cheng, Q., Russell, H., Sharpe, D., Kenny, F., and Qin, Q., 2001. GIS-based statistical and fractal/multifractal analysis of surface stream patterns in the Oak Ridges Moraine, Computer & Geosciences, v. 27, no. 5, p. 513-526.

Dietler, G. and Y. Zhang, 1992. Fractal aspects of the Swiss landscape. *Physica A*, 191, 213-219.

Fox, C. G. and D. E. Hayes, 1985. Quantitative methods for analyzing the roughness of the seafloor. *Rev. Geophys.*, 23, 1-48.

Gagnon, J.-S., S. Lovejoy and D. Schertzer, 2003. Multifractal surfaces and terrestrial topography. *Europhysics Letters*, 62, 6, 801-807.

Gallant, J. C., I. D. Moore, M. F. , 1994. Hutchinson and P. Gessler. Estimating fractal dimension of profiles: a comparison of methods. *Mathematical Geology*, 26, 4, 455-481.

Gibert, D. and V. Courtillot, 1987. Seasat altimetry and the South Atlantic geoid 1. Spectral analysis. *J. Geophys. Res.*, 92, B7, 6235-6248.

Gilbert, L. E. , 1989 .Are topographic data sets fractal? *PAGEOPH*, 131, 241-254.

Goodchild, M. F. , 1980. Fractals and the accuracy of geographical measures. *Mathematical Geology*, 12, 2, 85-98.

Herzfeld, U. C., I. I. Kim and J. A. Orcutt, 1995. Is the ocean floor a fractal? *Mathematical Geology*, 27, 3, 421-462.

Herzfeld, U. C. and C. Overbeck, 1999. Analysis and simulation of scale-dependent fractal surfaces with application to seafloor morphology. *Computers & Geosciences*, 25, 979-1007.

Huang, J. and D. L. Turcotte, 1989. Fractal mapping of digitized images: application to the topography of Arizona and comparisons with synthetic images. *J. Geophys. Res.*, 94, B6, 7491-7495.

Huang, J. and D. L. Turcotte, 1990. Fractal image analysis: application to the topography of Oregon and synthetic images. *J. Opt. Soc. Am. A*, 7, 6, 1124-1130.

Klinkenberg, B. and M. F. Goodchild, 1992. The fractal properties of topography: a comparison of methods. *Earth surface processes and landforms*, 17, 217-234.

Lavallée, D., S. Lovejoy, D. Schertzer and P. Ladoy, 1993. Nonlinear variability of landscape topography: multifractal analysis and simulation, in *Fractals in Geography*, edited by L. De Cola and N. Lam, pp. 158-192 , Prentice-Hall, New Jersey.

Leary, P., 1997. Rock as a critical-point system and the inherent implausibility of realiable earthquake prediction, *Geophys. J. Internat.*, *131*, 451-466.

Lewis, G. M., S. Pecknold, S. Lovejoy and D. Schertzer, 1999. The scale invariant generator technique for quantifying anisotropic scale invariance. *Computers and Geosciences*, 25, 9, 963-978.

Lilley, M., S. Lovejoy, K. Strawbridge, and D. Schertzer, 2004. 23/9 dimensional anisotropic scaling of passive admixtures using lidar aerosol data, Phys. Rev. E, 70, 036307-1-7.

Lovejoy, S. and D. Schertzer, 1990. Our multifractal atmosphere: A unique laboratory for non-linear dynamics. *Physics in Canada*, 46, 4.

Lovejoy, S., D. Lavallée, D. Schertzer and P. Ladoy, 1995. The $l^{1/2}$ law and multifractal topography: theory and analysis. *Nonlinear Processes in Geophysics*, 2, 16-22.

Lovejoy, S., D. Schertzer, Y. Tessier and H. Gaonac'h. , 2001b. Multifractals and resolution-independent remote sensing algorithms: the example of ocean color. *Int. J. Remote Sensing*, 22, 1191-1234.

Lovejoy, S. J.C. Mareschal, H. Gaonac'h, D. Schertzer, 2001. Anisotropic scaling models of the Earth's crust, mantle and surface gravity, Proc. of the European Geophys. Soc. General Assembly (Nice, France).

Mandelbrot, B. B. , 1967 . How long is the Coast of Britain? Statistical self-similarity and fractional dimension.

Science, 156, 636-638.

Mandelbrot, B. B. , 1975. Stochastic models for the Earth's relief, the shape and the fractal dimension of the coastlines, and the number-area rule for islands. *Proc. Nat. Acad. Sci. USA*, 72, 10, 3825-3828.

Mark, D. M. and P. B. Aronson, 1984. Scale-dependent fractal dimensions of topographic surfaces: an empirical investigation, with applications in geomorphology and computer mapping. *Mathematical Geology*, 16, 7, 671-683.

Okubo, P. G. and K. Aki, 1987. Fractal geometry in the San Andreas fault system. *J. Geophys. Res.*, 92, B1, 345-355.

Pecknold, S., S. Lovejoy, D. Schertzer, and C. Hooge,1997. Multifractal and resolution dependence of remotely sensed data: GSI and GIS, in *Scale in Remote Sensing and GIS*, edited by D. A. Quattrochi and M. F. Goodchild, pp. 361-394, CRC Press.

Perrin, J. *Les atomes*, NRF-Gallimard, Paris, 1913.

Richardson, L. F. The problem of contiguity: an appendix to statistics of deadly quarrels. *Gen. Syst. Yearb.*, 6, 139-187, 1961.

Schertzer, D. and S. Lovejoy, 1987. Physical modeling and analysis of rain and clouds by anisotropic scaling multiplicative processes. *J. Geophys. Res.*, 92, D8, 9693-9714.

Schertzer, D., S. Lovejoy, 1995. From scalar cascades to Lie cascades: joint multifractal analysis of rain and cloud processes. Space/time Variability and Interdependence for Various Hydrological Processes, Ed. R.A. Feddes, Cambridge University Press, p.153-173.

Schertzer, D. and S. Lovejoy , 1997. Universal multifractals do exist! *Journal of Applied Meteorology*, 36, 1296-1303.

Shiomi, K., H. Sato, and M. Ohtake, 1997. Broad-band power-law spectra of well-log data in Japan, *Geophys. J. Inter.*, *130*, 57-64.

Steinhaus, H. Length, 1954. shape and area. *Colloquium Mathematicum*, III, 1-13.

Tchiguirinskaia, I., S. Lu, F. J. Molz, T. M. Williams and D. Lavallée, 2000. Multifractal versus monofractal analysis of wetland topography. *Stochastic Environmental Research and Risk Assessment*, 14, 8-32.

Turcotte, D. L. , 1989. Fractals in geology and geophysics. *PAGEOPH*, 131, 171-196.

Turcotte, D. L. and E. R. Oxburgh, 1967. Finite amplitude convective cells and continental drift. *J. Fluid Mech.*, 28, part 1, 29-42.

Vening Meinesz, F. A. , 1951. A remarkable feature of the Earth's topography, origin of continents and oceans. *Proc. Koninkl. Ned. Akad. Wetensch.*, ser. B, 55, 212-228.

Weissel, J. K., F. P. Lincoln and A. Malinverno, 1994. The length-scaling properties of topography. *J. Geophys. Res.*, 99, B7, 13997-14012.

Xu, T., I. D. Moore and J. C. Gallant , 1993. Fractals, fractal dimensions and landscapes - a review. *Geomorphology*, 8, p. 245-262.